

Dynamic Pathway Selection Mechanisms of Brain Networks

Yanhui Chen, Yun Hu *, Jinhui Liu, Yu Wang and Aiting Li

National Demonstration Center for Experimental Electronic Information & Telecommunication Engineering Education, Xidian University, Xi'an 710071, China

* Correspondence: huyun@xidian.edu.cn

Abstract: Based on the dynamic reorganization mechanism of brain science and the fact that synaptic adaptability is affected by synaptic type, synaptic number and ion concentration, a bionic dynamic synaptic model is proposed and applied to a motif model and brain-like network model. By extracting the phase synchronization characteristics of the neural signals of node pairs in time sequence, and then deeply studying the regulation and control effect of synchronous discharge activities on effective links under the action of stimulating information, the path selection strategy is designed with the goal of maximizing the information transmission capacity between nodes. Four indicators are proposed: (1) pathway-synchronization-facilitation; (2) pathway-activation; (3) pathway-phase-selectivity; (4) pathway-switching-selectivity, which are used as the main basis for path selection in the network. The results show that the in-phase and anti-phase transition of neuron nodes under the action of time delay is an important way to form an effective link, and, in addition to the influence of synaptic strength and the number of central nodes on synchronization characteristics, the phase information carried by the stimulus signal also regulates the path selection. Furthermore, the paths between the pairs of stimulus nodes in the network have different phase preferences. In the brain-like network with twenty nodes, it is found that nearly 42% of the stimulus nodes have a strong phase preference; that is, the path can be selected and switched through the phase information carried by the information flow, and then the path with better representation information can be found. It also provides a new idea for how brain-like intelligences might better represent information.

Keywords: brain networks; neuron model; dynamic synaptic model; path selection strategy



Citation: Chen, Y.; Hu, Y.; Liu, J.; Wang, Y.; Li, A. Dynamic Pathway Selection Mechanisms of Brain Networks. *Appl. Sci.* **2023**, *13*, 296. <https://doi.org/10.3390/app13010296>

Academic Editors: Zheng Chang and Fani Pereira de Sousa

Received: 11 November 2022

Revised: 14 December 2022

Accepted: 19 December 2022

Published: 26 December 2022



Copyright: © 2022 by the authors. Licensee MDPI, Basel, Switzerland. This article is an open access article distributed under the terms and conditions of the Creative Commons Attribution (CC BY) license (<https://creativecommons.org/licenses/by/4.0/>).

1. Introduction

The intelligent information age is quietly changing people's way of life and the development mode of the world. It has become an important development trend to study the information transmission and representation of brain network in order to realize brain-like intelligence. Taking the simulation of brain connection mechanism as the starting point for the study of brain-like networks, in-depth study of the close relationship between information representation and loop selection is a hot topic in the study of brain-like intelligence. Recent studies have shown that the information representation of brain-like intelligent networks is mainly reflected by a variety of connection modes of the network; memory storage, extraction and forgetting in the brain network are all related to the link state between neurons [1,2]. Understanding the neural basis and working principle of brain networks by constructing bionic models and exploring the potential mechanism of loop selection and information representation in brain networks are of great significance to the development of brain-like intelligence.

In recent years, the study of the synapse has mainly focused on the perspective around the synapse. Ref. [3] investigates the release of synaptic vesicles as a random transfer model. The authors proposed a statistical model which focuses on the number of neurotransmitters released, and analyzes the plasticity of the complex signal transmission process of the chemical synapse. Ref. [4] states that the orientation of electrical synapses and dendritic positions and the synchronous activity between two neurons depend on electrical synapses

at different locations, and that this asymmetry affects information transmission at synapses and information processing by dendrites. Ref. [5] examines synapses that exhibit auto-adaptive properties when both chemical and electrical synapses are activated together, which can induce a transition from synchrony to desynchrony between neural circuits. In addition, Ref. [6] shows that the extracellular matrix (*ECM*) is an important composite protein to regulate brain development, brain connectivity and plasticity, and that *ECM* concentration is one of the important mechanisms in regulating the number of synapses so as to avoid excessive excitation of brain network changes. Ref. [7] explains that the dynamic changes in acetylcholine transmitter concentration can affect synaptic efficacy. This shows that synapse study by *ECM* concentration is being taken a new direction, which will be important in the understanding of information transmission in the brain.

Moreover, related studies have shown that the organization of brain networks is constantly optimized to achieve different tasks with a dynamic reorganization, and one of the mechanisms of dynamic reorganization present in the network is the presence of different neural rhythms (resonance, synchronization) in the processing of signals, while the dynamic reorganization induced by phase synchronization can be achieved by regulating the effective connectivity between nodes [8]. The results of [9,10] show that the basic functions of receiving, processing and transmitting information in the brain and the higher functions such as memory and association are directly related to the complex loops formed by synaptic coupling, and it can be said that the neural loop modulation mechanisms allow the brain to show different functional properties. Refs. [8,11] indicate that brain networks can exhibit complex loop connections regardless of whether the brain is in a resting or task state; thus, they choose different network paths to achieve functional tasks, such as memory, association and decision making. In this paper, both dynamic synapses and correlations assessment are mainly considered in terms of how dynamic reorganization of the network can flexibly adapt to changes in functional coupling to external stimuli. In this mode of synchronization, features that can be enhanced or diminished by the phase information of stimulus signals can be used as an effective connection mechanism for dynamic network reorganization.

The research content and main contributions of this paper are as follows: in the Section 1, the research background and significance of the article are expounded in detail; in the Section 2, according to the latest brain science research results, the bionic dynamic synapses are constructed by combining the electrical synaptic model, chemical synaptic model and synaptic number model under the influence of concentration; in the Section 3, the bionic dynamic synapses are applied to the neural network and the effect of stimulation information phase offset on path selection in the network is explored. The main contributions of this paper are as follows: (1) we propose a bionic dynamic synaptic model under the influence of concentration and apply it to doubly coupled nervous system and neural networks with small world network characteristics; (2) we use the original model to study the close relationship between phase synchronization and effective links, propose a path selection method based on information flow disturbance and prove that there is a moderating relationship between the path selection mechanism and the phase difference of stimulus information in the network.

2. Materials and Methods

The synapse is not only an important part of the brain network, but also the key to the realization of information transmission, information representation, perceptual decision-making and other functions. The connection between neurons is made up of chemical synapses or electrical synapses, even the coexistence of electrical synapses and chemical synapses, and they interact with each other in the process of information transmission, together affecting the response ability of the system [12]. In addition, synaptic structures with complex biological characteristics play an important role in regulating signal transmission in the nervous system. With the development of brain science and observation technology, the influencing factors of biological synapses have been deeply understood. Ref. [6] shows

that *ECM* is an important compound protein regulating brain development and brain connection and plasticity, and that *ECM* concentration is one of the important mechanisms for regulating the number of synapses, which can dynamically regulate synaptic efficiency so as to avoid the over-excitation of the brain network and cause physiological diseases. Therefore, this paper takes the effect of concentration on synapses as a new research direction, which will play an important role in developing in-depth understanding of brain information transmission [13–15].

With the in-depth study of bionic networks, it is found that information representation is closely related to the choice of neural loop, so the study of synaptic structure plays an important role in neural loops and even in the nervous system. In addition, there are many forms of synapses in the neural network, and the connections of different synaptic structures will lead to different neural loops. Therefore, by exploring the complex mechanism of synapses and constructing dynamic synapses in accordance with biological characteristics, it is a breakthrough to realize brain-like networks. Based on the above research results, this study deeply understands the dynamic effects of synapses on neural activity, comprehensively considers the synaptic quantity regulation mechanism under the influence of synaptic type and *ECM* concentration, constructs a biomimetic dynamic synaptic model and constructs a neuron system based on this model. The neuron model and dynamic synaptic model are as follows.

2.1. Neuron Model

In order to strike a balance between biological authenticity and computational efficiency, we apply the dimensionless Izhikevich neuron model, which simplifies the amount of computation while retaining the real biological dynamic characteristics. It can be used as the basic unit of the network model. The subthreshold dynamic equation of the membrane potential of any neuron node *i* in the network follows the differential equation shown in the Equation (1):

$$\begin{cases} \frac{dv_i(t)}{dt} = 0.04v_i^2(t) + 5v_i(t) + 140 - u_i(t) + I_i(t) + I_i^{syn}(t) \\ \frac{du_i(t)}{dt} = a(bv_i(t) - u_i(t)) \\ \text{if } v_i \geq 30 \text{ mV} \\ \text{then } \begin{cases} v_i(t+1) \rightarrow c \\ u_i(t+1) \rightarrow u_i(t) + d \end{cases} \end{cases} \quad (1)$$

where $v_i(t)$, $u_i(t)$ represent the membrane potential of the neuron *i* and the recovery voltage of the neuron *i* in the network, respectively, and $I_i(t)$ represent the external input current of the neuron *i*. $I_i^{syn}(t)$ indicates that the neuron *i* is subjected to a dynamic postsynaptic current. Parameters *a* and *b* represent the speed of neuronal recovery voltage and the degree of neuronal excitability, respectively. The greater the *a* value, the faster the recovery speed of the membrane voltage $v_i(t)$, and the greater the *b* value, the easier it is for the neuron to excite and produce nerve impulses. The parameters *c* and *d* represent the reset values of the membrane voltage $v_i(t)$ and the recovery voltage $u_k(t)$ after the neuron emits the pulse. When the membrane voltage $v_i(t)$ is higher than the activation threshold 30 mV, the membrane voltage $v_i(t)$ and recovery voltage $u_k(t)$ should be reset to ensure the biological characteristics of the neuron model.

For Izhikevich neurons, by changing the values of parameters *a*, *b*, *c* and *d*, the model can simulate common nerve pulses such as regular spiking, intrinsically bursting, fast spiking and so on. The Izhikevich parameters are shown in Table 1.

Table 1. Parameter tables of six typical Izhikevich neurons.

Izhikevich Neuronal Pulse Type	a/ms^{-1}	$b/10^{-9}\Omega^{-1}$	c/mV	d
Regular Spiking	0.02	0.2	−65	8
Intrinsically Bursting	0.02	0.2	−55	4
Fast Spiking	0.1	0.2	−65	2
Low-threshold Spiking	0.02	0.25	−65	2
Resonator	0.1	0.26	−65	2
Chattering	0.02	0.2	−50	2

2.2. Dynamic Synaptic Model

The synapse is an important part of the nervous system, and neurons transmit signals through synaptic structures. In the process of information transmission, mixed synapses have a certain effect on signal transmission, and the number of synapses between neurons will also affect the response ability of the nervous system. Therefore, taking into account the respective advantages of chemical synapses and electrical synapses, this section constructs a bionic dynamic synaptic model according to the proportion of chemical synapses and electrical synapses and the regulation of ECM concentration on the number of synapses.

(1) Electrical synaptic coupling takes into account the fast channel of ion exchange between neurons. $I_{i,e}^{syn}$ represents the current of the neuron after the electric synapse, as shown in its Equation (2):

$$I_{i,e}^{syn} = \sum_j g_e^{syn} A(i, j) (V_i - V_j) \tag{2}$$

where g_e^{syn} is the electrical conductivity of the electrical synaptic channel, $A(i, j)$ represents the coupling relationship between neuron i and neuron j , V_i and V_j represent the membrane potential of neuron i and neuron j , $A(i, j) = A(j, i) = 1$, indicating that there is a coupling between the neuron i and the neuron j . $A(i, j) = A(j, i) = 0$ means that there is no coupling between neurons.

(2) Chemical synaptic coupling takes into account the direction of transmission of pre-and post-synaptic neurons and the release process of neurotransmitters. $I_{i,c}^{syn}$ represents the post-synaptic current of neurons i , as shown in (3):

$$I_{i,c}^{syn} = \sum_j g_c^{syn} A(i, j) S_j (V_i - V_{syn}) \tag{3}$$

where g_c^{syn} is the coupling strength of chemical synapses, $A(i, j)$ is expressed as the coupling relationship between neuron i and neuron j and V_{syn} is the reverse potential of neurons which determines the type of synapse: $V_{syn} = 0$ means excitatory postsynaptic potential (EPSP); $V_{syn} = -1.2$ represents inhibitory postsynaptic potential (IPSP). The release process of chemical synaptic vesicles is measured by S_j , which is determined by the membrane voltage V_j , as shown in (4):

$$\frac{dS_j}{dt} = \frac{\alpha(V_j)(1 - S_j)}{\varepsilon} - \frac{S_j}{\tau_{syn}} \tag{4}$$

where $\tau_{syn} = 1/\delta$ is the synaptic decay rate. When the neuron is in the resting state ($V_j < 0$), S_j decreases slowly and $dS_j/dt = -S_j/\tau_{syn}$; when $V_j > 0$, $S_j \rightarrow 1$ jumps rapidly to 1.

Presynaptic neurons act on postsynaptic neurons only when S_j changes rapidly, which is different from the rapid coupling of electrical synapses. $\alpha(V_j)$ is the synaptic recovery equation, such as Equation (5):

$$\alpha(V_j) = \frac{\alpha_0}{1 + e^{(-V_j/V_{shp})}} \tag{5}$$

where $\alpha(V_j)$ is the Heaviside equation that models the mechanism of chemical synaptic vesicle release.

(3) According to the latest microbiological research [16,17], the number of synapses will be affected by the concentration of ECM, thereby regulating the synaptic efficiency. Therefore, we will build the synaptic number model $N[C]$ under the influence of concentration. The specific expression form is shown in Equation (6):

$$N[C] = N[C] + \text{int}(2^C) \tag{6}$$

where $N[C]$ denotes the number of synapses under the influence of concentration and C denotes the concentration time function after external stimulation. $\text{int}(\cdot)$ is the rounding function.

Considering the cell growth pattern, we use power functions to describe the growth rate of the number of synapses. In addition, based on the concentration environment in which the neuron is located [18,19], and with the concentration continuously iterated with the external stimulus I_{ext} , the specific expression is shown in Equation (7):

$$C(t) = C(t) + \alpha I_{ext} \tag{7}$$

where $C(t)$ denotes the concentration function, which is influenced by the external stimulus current I_{ext} , and α denotes the amount of change after receiving the concentration.

The parameters C_L and C_H are used to indicate the minimum concentration threshold and the maximum concentration threshold; when the ECM concentration is placed between C_L and C_H , it indicates that the connections between neurons are in the appropriate concentration space, and the number of synapses will grow with the concentration until it grows to the maximum number of synapses after which the concentration starts to decrease, ensuring the growth pattern of the organism. The concentration recovery function is shown in Equation (8):

$$C(t) = C(t) - D \tag{8}$$

where D denotes the coefficient of decrease in ECM concentration after saturation of synaptic number.

When the concentration of ECM exceeds C_H , it means that the concentration space of the neuron is beyond the tolerance range, and the neuron turns on its self-protection mechanism. Then, the ECM concentration begins to decrease, resulting in a change in the number of synapses, which follows Equations (9) and (10):

$$C(t) = C(t) \cdot \exp\left(-\frac{1}{M}\right) \tag{9}$$

$$N[C] = \text{int}(\beta C). \tag{10}$$

Equations (8) and (9) denote the ECM concentration recovery function and the synapse number change function, respectively. M represents the concentration cooling coefficient and β represents the effect of concentration on the number of synapses.

Based on the above studies, this paper comprehensively considers the number of electrical synapses and chemical synapses and the number of synapses affected by concentration and constructs a dynamic synaptic model. I_i^{syn} represents the dynamic postsynaptic current acting on the neuron i . The expression is as shown in (11):

$$I_i^{syn} = N[C] \sum_j A(i, j) \left\{ g_e^{syn} p(V_i - V_j(t - \tau)) + g_c^{syn} (1 - p) S_j(t - \tau) (V_i - V_{syn}) \right\} \tag{11}$$

where g_e^{syn} denotes the electrical synaptic strength, g_c^{syn} denotes the chemical synaptic strength, $A(i, j)$ denotes the synaptic coupling between neuron i and neuron j , $V_i (i = 1, 2, \dots, N)$ denotes the membrane voltage value of neuron, V_{syn} denotes the reverse electrical potential

present at chemical synapses, which is used to distinguish the type of synapses, and p denotes the percentage of electrical synapses. $p \rightarrow 1$ indicates that the percentage of electrical synapses between neurons gradually increases, while the percentage of chemical synapses decreases. S_j denotes the series of biological responses of chemical synapses [20–25].

2.3. Motif Connection Model

The complexity of the brain network makes it difficult for researchers to explore and imitate the working mechanism of the neural network. In recent years, related studies have shown that the motif model in complex brain networks is the basic unit module of the complex network model. The proposal of the motif model enables researchers to start with the simple network composed of the motif model and deeply study the relevant characteristics between the network nodes. This plays a very important role in the study of the nature and function of the whole network. At present, the idea of research based on the motif model is widely used in the exploration of complex networks and has achieved important scientific research results, which is very enlightening. Therefore, in the research of effective links between network nodes, it is necessary to explore the relationship between effective links and node synchronization from the typical motif model [26–28].

Based on the above considerations, we construct a motif model network based on dynamic synapses. It can be seen from Figure 1a that the coupling mode between the two neurons is relatively fixed, but when there are three neuron nodes, the connections between them can evolve a variety of connection states (only four types are listed in this figure), as shown in Figure 1b. The interaction between neurons under different structural connections makes them show rich network dynamics, which should be the characteristics of brain-like networks. Therefore, we rely on the motif model of Figure 1 to analyze the relationship between effective link and synchronization state in order to prepare for the follow-up exploration of the path selection mechanism in multi-node networks.

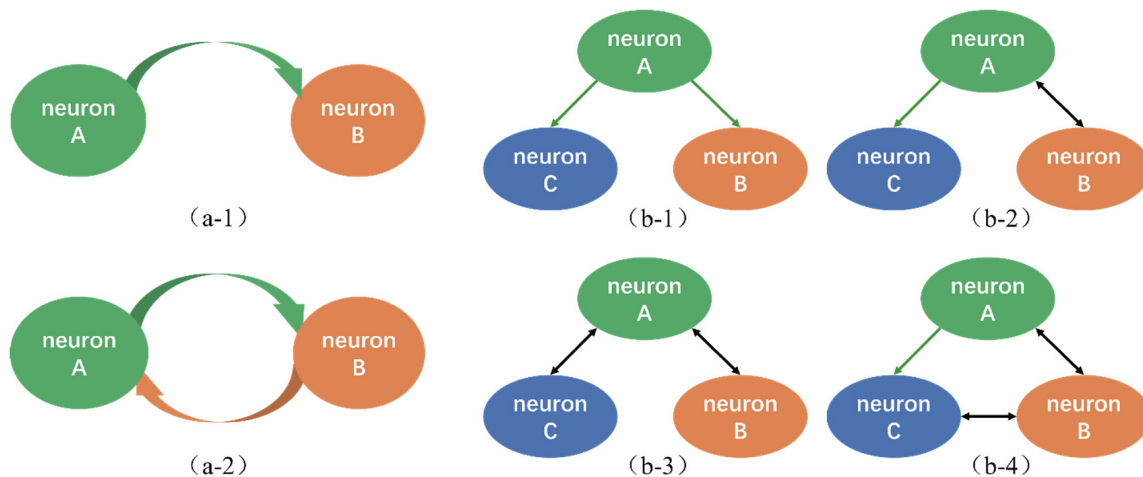


Figure 1. Schematic diagram of motif model connection ((a-1): Unidirectional coupling of neurons A and B. (a-2): Dual coupling of neurons A and B. (b-1): Unidirectional coupling of neurons A and B, Unidirectional coupling of neurons A and C. (b-2): Dual coupling of neurons A and B, Unidirectional coupling of neurons A and C. (b-3): Dual coupling of neurons A and B, Dual coupling of neurons A and C. (b-4): Dual coupling of neurons A and B, Unidirectional coupling of neurons A and C, Dual coupling of neurons B and C.).

Phase synchronization is common in oscillatory systems, especially in the study of brain networks in recent years, and electroencephalogram recording and magnetoencephalogram experiments have proved that synchronization plays an important role in information transmission and the representation of brain networks. This is because we use phase synchronization to study the indicators of effective transmission. Taking the motif model of two neurons in Figure 1a as an example, the phase synchronization analysis is

evaluated by the pulse discharge sequence of the neuron, i.e., $\varphi(t) = |\phi_A(t) - \phi_B(t)| \leq Z$ where $\phi_A(t)$ and $\phi_B(t)$ are the instantaneous phases of the neural node A and the neural node B at time t , and Z is a constant. The analysis of phase synchronization is mainly divided into two steps:

(1) Extract the instantaneous phase from the signal.

There are many methods of phase locking [29], we use the classical Hilbert transform to obtain the instantaneous phase of the signal. The resolved signal $\varepsilon(t)$ is a complex function of the continuous time variable $x(t)$ in the form of Equation (12):

$$\varepsilon(t) = x(t) + ix_h(t) = a\varepsilon(t)e^{i\Delta\phi(t)} \tag{12}$$

where $\varepsilon(t)$ and $\phi(t)$ are the instantaneous amplitude and phase of the signal $x(t)$ resolution signal, and the instantaneous phase for the neuron A is obtained from the signal $x(t)$ of the input neuron A . $x_h(t)$ is attained through the signal $x(t)$ Hilbert transform [30–32].

(2) Phase locked quantization.

For an independent time-series $x(t)$, the distribution of relative phases is uniform within a given time window T . There are various schemes for the detection of phase locking which can quantify the degree of uneven relative phase distribution. We use phase coherence to measure the synchronous state (phase coherence, PC) as the quantitative index of the phase of two neurons over a period of time, the specific expression is (13):

$$PC(n_i, n_j, \Delta\varphi) = \frac{1}{T} \sum_{t=1}^T e^{i\Delta\varphi(t)} \tag{13}$$

where T denotes the size of the time window function and $\Delta\varphi(t)$ denotes the phase offset of a pair of stimulus nodes n_i and n_j at the time of t . When the stimulus nodes n_i and n_j are in the fully synchronized phase, PC takes the value of 1; when they are not fully synchronized, PC takes the value of 0, i.e., $PC \in [0, 1]$. For each neuron node, the PC value can be calculated, and the resulting PC is the average phase coherence over multiple time windows PC . This allows the quantification of the PC values of all nodes in the entire network, which in turn measures the ability and effective links of information transmission between nodes.

Equation (13) represents the synchronization index of information transmission between stimulating node pairs, but the transmission delay between nodes will also affect the synchronization state of nodes. Therefore, we give the pathway-synchronization-facilitation index (PSF). This measures the change range of PSF between node pairs under the action of phase offset of stimulus information, which plays an important role in exploring the path selection mechanism scientifically in this study. $PSF(n_i, n_j)$ denotes the pathway-synchronization-facilitation index of node n_i and node n_j . The specific expression is (14):

$$PSF(n_i, n_j) = \max_{[0, 2\pi]}(PC(n_i, n_j, \Delta\varphi)) - \min_{[0, 2\pi]}(PC(n_i, n_j, \Delta\varphi)) \tag{14}$$

where $PC(n_i, n_j, \Delta\varphi)$ is denoted as the coherence value of node n_i and node n_j under the condition that the stimulated phase offset is $\Delta\varphi$. $PSF(n_i, n_j)$ quantifies the fluctuation range of the coherence values under the interaction between two nodes n_i and n_j under a fixed phase offset condition.

$PSF(n_i, n_j)$ is used to measure whether the change in synchronization strength between node pairs is correlated with the phase information carried by the external stimulus. After theoretical analysis, if the PC values between node pairs (n_i, n_j) vary widely under different phase conditions, it indicates that the PSF of this pair is more active, i.e., PSF is higher, and that it is more sensitive to the phase information carried by the stimulus information and is more easily affected by the phase.

To sum up, this paper utilizes Izhikevich neurons to form the motif model in Figure 1. The connection between any two neurons uses dynamic synapses, and $I_k(t) = a\sin(2\pi f(t + \Delta\varphi))$

is applied to each neuron node as the input signal of external disturbance. $\Delta\varphi$ represents the phase carried by the input information, and its value range is $[0, 2\pi]$. On this basis, the influence of the phase information carried by the stimulus information in the brain network on the synchronization characteristics and effective links in the network are investigated in this work.

3. Results

This section mainly elucidates that, when neurons are connected to each other to form the motif model of Figure 1, and when a pair of neuronal nodes are driven by external stimuli, the synchronization state under discharge activity is studied. Different types of motif models will be analyzed below.

3.1. Two Motif Models

By constructing the motif model of two neurons based on dynamic synapse, the synchronization phenomenon and effective link in the network are studied. The neuron node is driven by external stimulus and its amplitude intensity is $a = 1$. The signal frequency is $f = 11$ Hz. The discharge sequence between two neurons in different coupling connection states and the statistical distribution of two neurons in the connection state are shown in Figures 2 and 3, respectively.

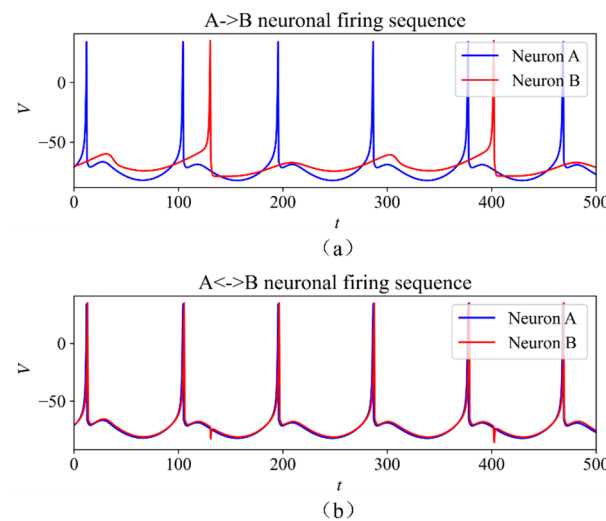


Figure 2. Two neuronal discharge sequences (a) Neurons A and B are unidirectional coupling; (b) Neurons A and B are dual coupling.).

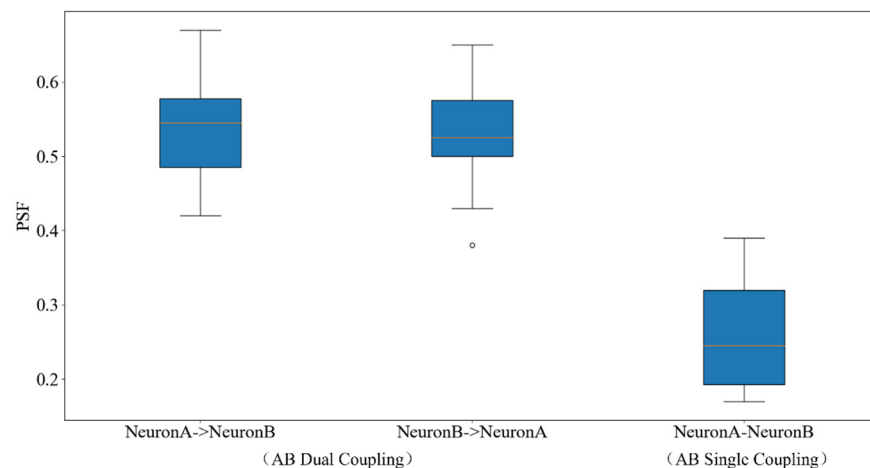


Figure 3. PSF boxplots for the different coupling states.

Figure 2 shows the discharge sequence between two neurons with different coupling connections. Figure 2a shows that, in the unidirectional coupling state, such as the structure of Figure 1(a-1), discharge sequence between neurons demonstrates a lack of consistency, and the synchronization activity between neuron *A* and neuron *B* is weak. This is because there is only one-way action between neurons and there is no feedback link. When the neurons are in the state of two-way coupling connection (i.e., feedback link exists), as shown in Figure 1(a-2) structure and the discharge sequence shown in Figure 2b, it can be seen that the discharge sequences between neurons are highly consistent and the pulse sequences coincide at a fixed time. This phenomenon is called isochronous synchronization.

Figure 3 is a box-line plot that quantitatively portrays the values of the *PSF* taken under different coupling connections. The upper and lower limits of the bins each indicate the upper and lower quartiles, the entire box indicates the dispersion of the *PSF* and the line in the middle indicates the median of the dataset. Through running the experimental data 100 times, Figure 3 quantitatively describe the values under different coupling connections. For the dual coupled motif model, the *PSF* exponent is higher, i.e., it shows that it is more sensitive to the phase information carried by the input information. For the single coupling model, the *PSF* value is around 0.28. The smaller *PSF* value indicates that the phase carried by the input information has less impact on it under this structure, i.e., the synchronization of the nodes is less affected when the stimulus information changes the carried phase, which, in turn, cannot regulate the effective links in the network.

In the brain network, the *PSF* is affected not only by the phase shift of the stimulus, but also by the time delay. Therefore, this study considers the transmission delay between transmission paths and describes the effect of delay on the *PSF*. The simulation is shown in Figure 4.

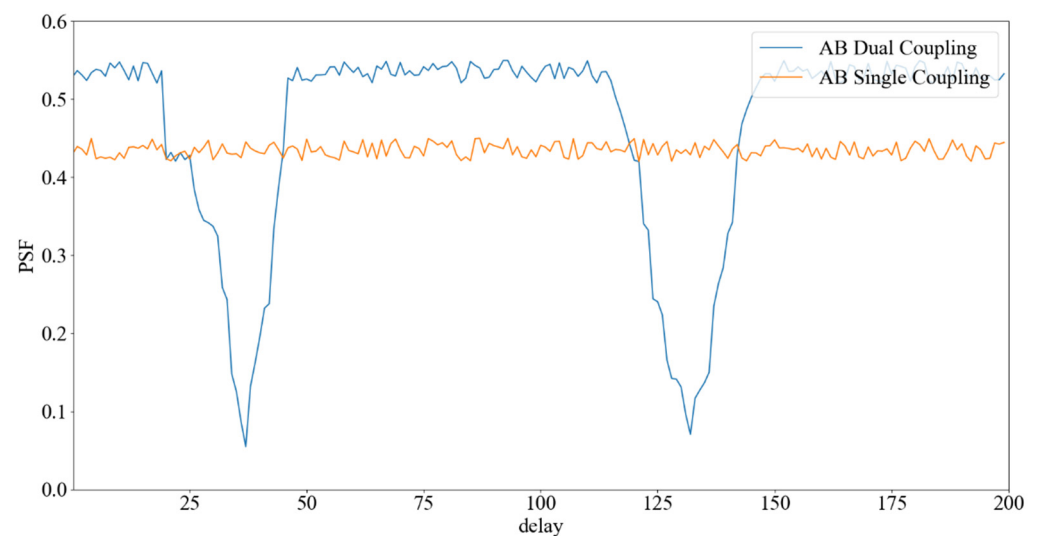


Figure 4. Effect of time delay of two motif model on *PSF*.

Figure 4 represents the *PSF* effect under the time delay scale of [0, 200]. From Figure 4, it is seen that the *PSF* value under single coupling fluctuates around 0.43 and does not change significantly with the increase in time delay, indicating that the phase information carried by the stimulus phase has less ability to regulate under the single coupling structure under the influence of time delay, and its coherence value *PC* is more stable. In bidirectional coupling, the *PSF* value has a strong fluctuation between [0.1, 0.52]. With the increase in time delay, the *PSF* value appears to show a trend of in-phase and inverse-to-phase changes, which shows that the synchronization of neural nodes can be regulated in-phase or inverse-to by means of time delay [17–19]. Therefore, exploring the effect of time delay on *PSF* between coupled nodes is important to investigating the relationship between stimulus information phase shift and the selection mechanism of network paths.

3.2. Three Motif Models

In the previous section, the synchronization status of different structural links under the two motif models is analyzed, and it is concluded that the connection structure and transmission delay have influence on the synchronization characteristics. Because the structure of the three motif models is changeable, but their essence is the extension of the two motif models, the analysis of the three motif models in Figure 1b mainly considers the synchronization state between the links of the motif model and the effective links when the structural links are missing. Therefore, we next focus on the motif model of Figure 1(b-2,b-3) in order to analyze the synchronization state and effective link under this link.

Figure 1(b-2) structure is a connection model in which neuron C is inserted between doubly coupled neurons A and B. From the physical structure neuron C is directly regulated by neuron A and indirectly regulated by neuron B. Its discharge sequence and the PSF distribution are shown in Figures 5 and 6.

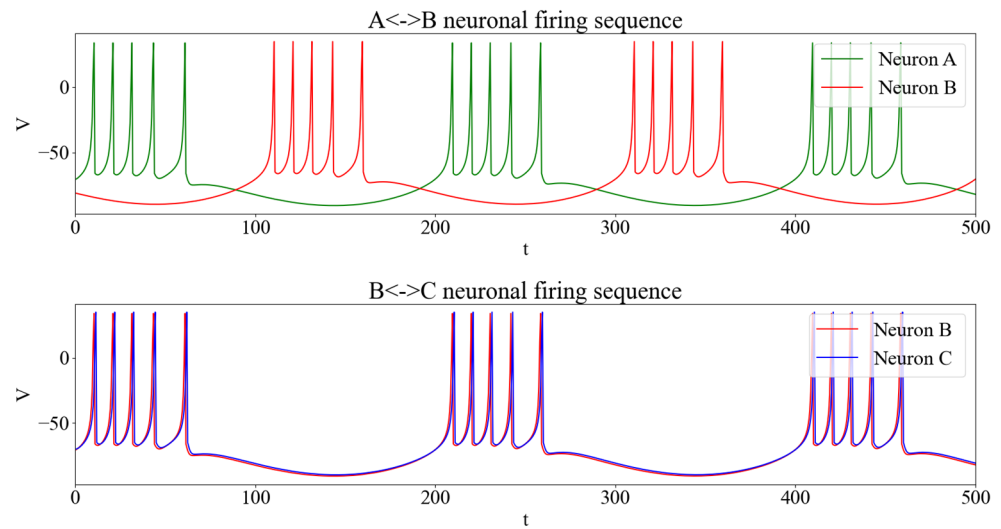


Figure 5. The discharge sequence of three neurons connecting model 1(b-2).

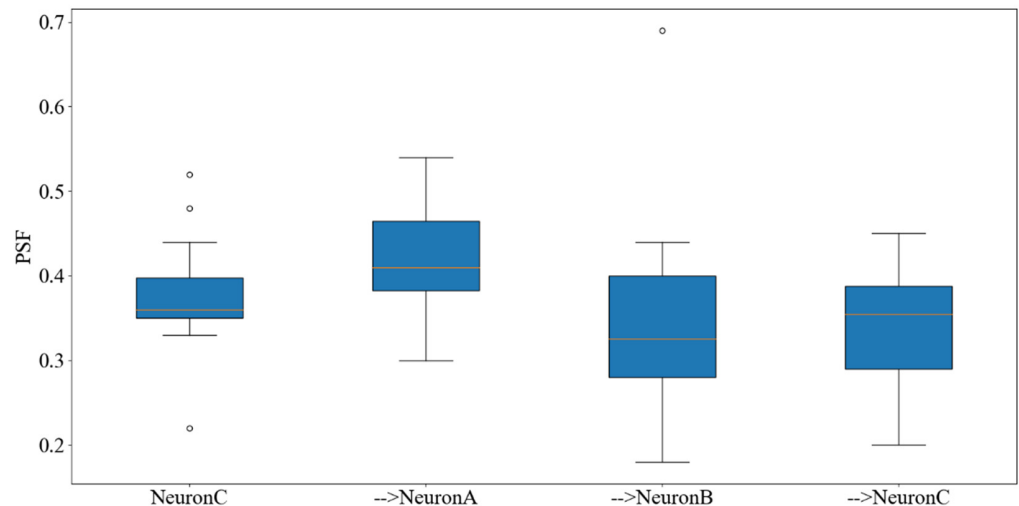


Figure 6. PSF distribution diagram of three neurons model 1(b-2) in different connection States.

Figure 5 is a discharge sequence for three motif models. Its analysis method is similar to that of two motif models. However, in Figure 5, the discharge sequence diagrams of neurons with structural links (neuron A and neuron B) and without structural links (neuron B and neuron C) are simulated, respectively. It can be seen from Figure 5 that there is a certain difference in the pulse sequence between neuron A and neuron B, but their

discharge activities are regular and consistent. Although there is no structural link between neuron *B* and neuron *C*, there is a phase synchronization state in the discharge sequence, which is consistent with the theoretical analysis. This shows that the synchronization state between neurons is an important means of neural information transmission. Therefore, it can be shown from Figure 5 that there is an effective transmission between neuron *B* and neuron *C* in the process of information transmission; synchronization characteristics can build dynamic effective links between neurons and these effective links do not necessarily correspond to structural links one by one, which may be the main reason for flexible path switching in brain networks.

Figure 6 is a boxplot of the three Motif models. It also conducted 100 simulation experiments, and the statistical analysis concluded that the *PSF* values between neurons $C \rightarrow A \rightarrow B \rightarrow C$ are relatively stable. The *PSF* value is maintained between [0.3, 0.4]. Under this structure, the phase information of the stimulus signal has a certain promoting effect on the synchronous state, thus resulting in a “new” connected pathway *BC*. The simulation results show that there is an effective pathway between the neuronal nodes, that the synchronization between the neural nodes can be regulated by the phase offset of the stimulus signal and that the degree of regulation depends on the size of the *PSF* value.

Under the model structure of Figure 1(b-2), it also considers the effect of time delay on *PSF*. The simulation results are shown in Figure 7. The value range of delay is [0, 160]. Through the analysis of the simulation results, it is found that, compared with the two neuron structure links, the *PSF* of Figure 1(b-2) model is lower. It is maintained between [0.28, 0.36] and there is a weak fluctuation phenomenon with the increase in time delay, indicating that the time delay also has a certain effect under this structure. In addition, the reason for the small change trend of *PSF* is that the increase in the number of central nodes affects the transmission of nerve impulses in the whole link, and the signal is annihilated in the bottom noise of the nervous system in the process of transmission due to the increase in the number of nodes. Therefore, the future multi-node in-depth study will consider the impact of the number of central nodes on *PSF*.

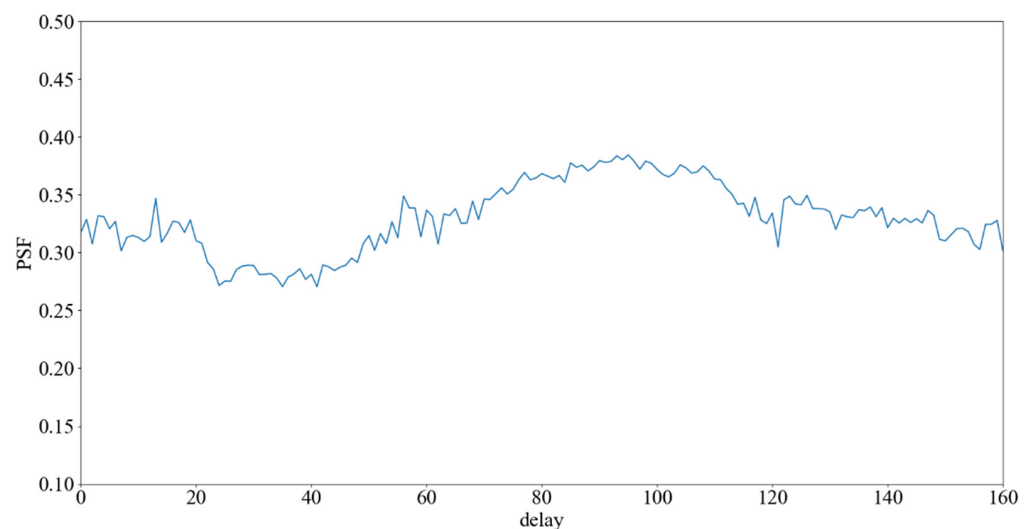


Figure 7. Effect of time delay on *PSF* in three neurons model 1(b-2).

In order to more comprehensively study the synchronization and effective link between the three motif models, we next simulate and analyze the motif model of Figure 1(b-3). Figure 1(b-3) is based on Figure 1(b-2); a structural link is added between neuron *A* and *C* to form a double coupling between neuron *A* and *C* (with feedback link). The discharge sequence and *PSF* statistical diagrams of the structure of Figure 1b-3 are shown in Figures 8 and 9, respectively.

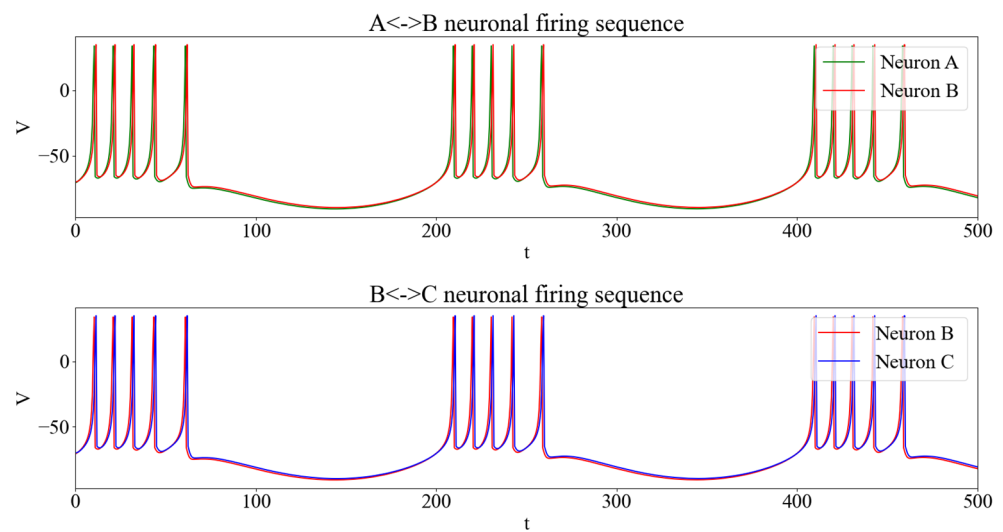


Figure 8. The discharge sequence of three neurons connecting model 1(b-3).

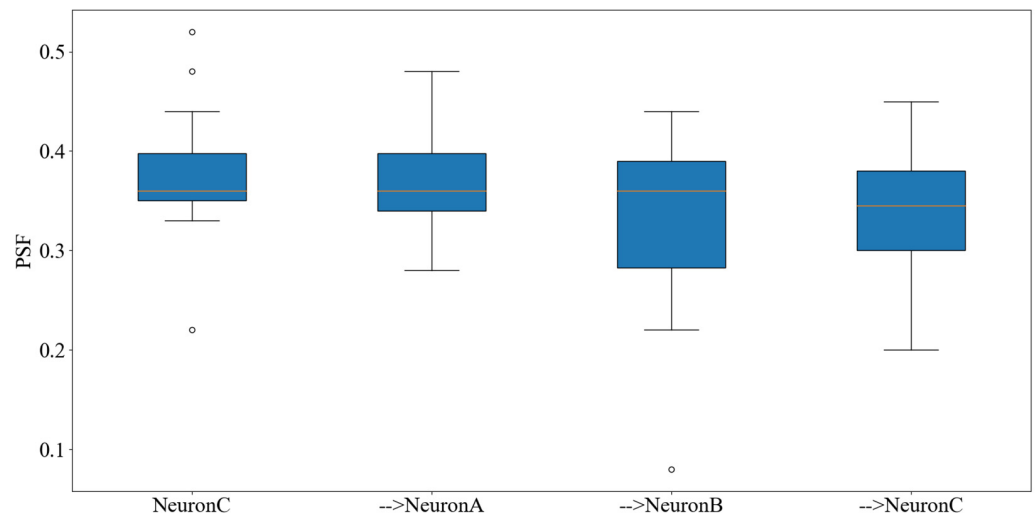


Figure 9. PSF distribution diagram of three neurons model 1(b-3) in different connection States.

Figures 8 and 9 show discharge sequences and *PSF* statistical diagrams of the motif model of Figure 1(b-3), respectively. According to the consistency of the discharge sequence between neurons in Figure 8, no matter whether there is a structural link between neurons—for example, there is a structural link between neurons *A* and *B*, and there is no structural link between neurons *B* and *C*—neurons achieve isochronous synchronization in the firing process; that is, an effective link is formed between any two neuron nodes. In addition, it can be seen that the *PSF* data distribution in the box diagram of Figure 9 is more stable than that of Figure 6, but the fluctuation of the *PSF* value of neuron *C* is more obvious from the box diagram, indicating that it is more easily regulated by the phase information of stimulus signal. Therefore, it is found that the synchronization between neural nodes is an important index to form an effective link, and the synchronization between neurons is regulated by many factors.

The relationship between the *PSF* and the transmission delay of motif model 1(b-3) is shown in Figure 10. It can be seen that the value of *PSF* changes obviously with the increase in delay, and that its value fluctuates greatly in the range of [0.22, 0.38]. This indicates that the stimulus node is more vulnerable to in-phase or out-of-phase stimulation; that is, it is more sensitive to the phase information of external stimulus signal. In addition, it can be seen that when the delay is in the range of [0, 160], the *PSF* value changes periodically with the change of delay, which reflects that the information transmission between nodes

is related to phase locking. In this structure, *PSF* will dynamically adjust the intensity of synchronization with the size of the time delay, so that the synchronization between nodes has a dynamic change, and then affect the connection state of effective links in the network. This indicates that the brain network can reorganize nodes in different time dimensions with synchronous state, and then achieve a variety of effective links to facilitate task efficiency.

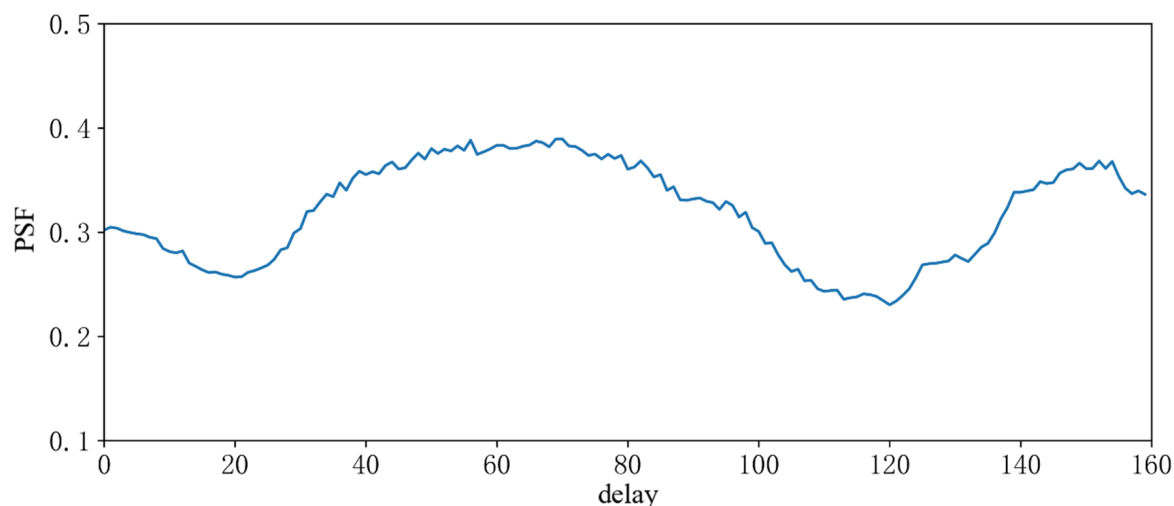


Figure 10. Effect of time delay on *PSF* in three neurons model 1(b-3).

3.3. Regulation of Path Selection by Different Phases of Stimulus Signal

For the study of the motif model, it can be found that in the motif model with two or three nodes connected to each other, the synchronization between nodes shows a complex dependence on the phase offset and transmission delay of the stimulus signal. Therefore, in order to extend the analysis to the more complex network model, we next construct a network model with 20 delay nodes to simulate the brain, and each network node is a neuron group of a small-world network with 100 neuron nodes. In addition, there is a double coupling state between the nodes.

Figure 11 shows the schematic diagram of the relationship between the *PSF* values of some nodes and the central nodes. It can be seen that the *PSF* values of the stimulus node pairs (X, Y) are different between the paths passing through one central node and those passing through two nodes, which indicates that there is a certain relationship between the path choice between the stimulus information pairs and the number of central nodes. Therefore, the box diagram of Figure 12 is used to describe the influence of the number of central nodes on the *PSF* index between node pairs. As can be observed from the boxplot, when and only when there is one pivot node, its *PSF* value is distributed in $[0.03, 0.08]$. As the number of pivot nodes increases, the value of *PSF* and the distribution interval increases; when the number of pivot nodes is four, the value of *PSF* is distributed between $[0.05, 0.13]$, indicating that the data of *PSF* fluctuates more, but when the number of pivot nodes is five or the number of pivot nodes is greater than five, the value of *PSF* decreases and the fluctuation range becomes smaller. From the perspective of the significance of *PSF*, when the number of hub nodes increases to a certain number, the *PSF* values between nodes in the network can be regulated by the phase shift of the stimulus information. This shows that the path selection strategy in the network is affected not only by the phase of stimulus information, but also by the number of central nodes. Therefore, in the complex link structure composed of twenty nodes, limiting the maximum number of central nodes to five, which means that the path of up to six nodes is mainly searched in the path search, and 95% confidence interval is used for evaluation.

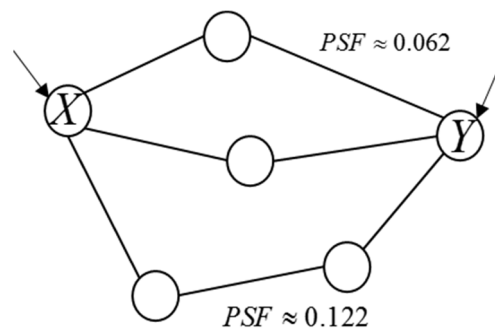


Figure 11. The schematic diagram of the central node.

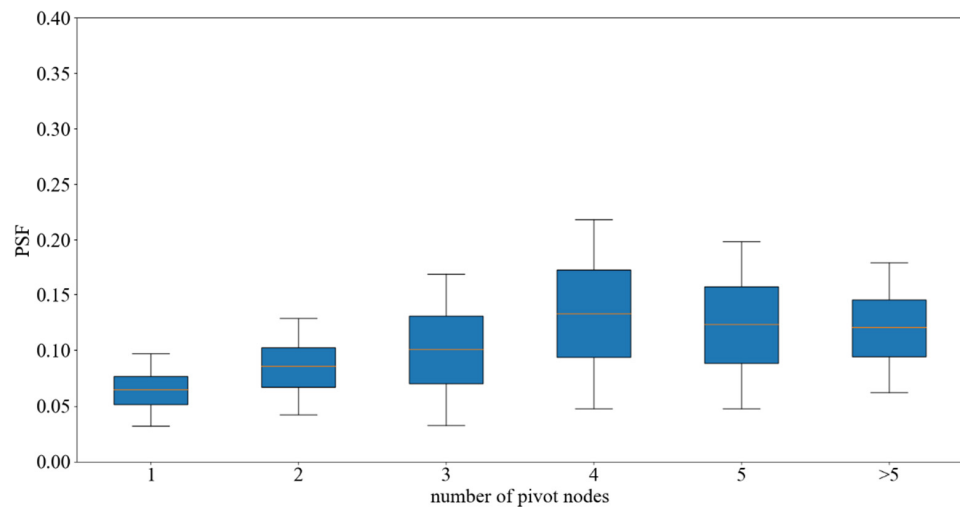


Figure 12. Boxplot of the number of central nodes regarding the PSF.

In addition to the number of central nodes, the synaptic strength g^{syn} of node pairs also plays an important role in synchronization characteristics. By obtaining the PSF values at different synaptic strengths g^{syn} , it can be found that there is a close relationship between the effective link between stimulated nodes and the synaptic strength. By fitting the data, there is a high degree of coherence between the PSF values ($PC = -0.72, p < 0.003$) at different strengths and different nodes. In addition, it can be seen by the simulation results in Figure 13 that as the synaptic strength g^{syn} increases, PSF value becomes smaller and smaller, which indicates that when the coupling strength between the nodes gradually increases, resulting in a strong structural link between the nodes, it is more difficult to regulate the synchronization between the nodes using the phase information of the stimulus information. This indicates that there should be a general weak coupling phenomenon between the nodes of the brain network.

In order to evaluate the path transmission capability between a pair of excited nodes in the network, the model gives the proposed metric of the degree of activation of an effective path and the degree of interaction between pairs of information transmission nodes at a given stimulus phase offset $\Delta\varphi$, given the physical link determination. It is assumed that $P_{1,n}(i = 1, 2, \dots, n)$ is denoted as the set of all paths between node pairs (n_1, n_n) , thus setting the maximum activation state (pathway activation, PA) of a path through $\Delta\varphi$ pivot nodes at a stimulus phase offset of $n - 1$. $PA(n_1 \dots n_n, \Delta\varphi)$ denotes the coherence of a path between a pair of stimulus node pairs (n_1, n_n) after passing through different pivot nodes, which measures the transmission capability of the whole path or the degree of effective path activation and is defined as Equation (15):

$$PA(n_1 \dots n_n, \Delta\varphi) = \prod_{i=1, \dots, n-1} (PC(n_i, n_{i+1}, \Delta\varphi)). \tag{15}$$

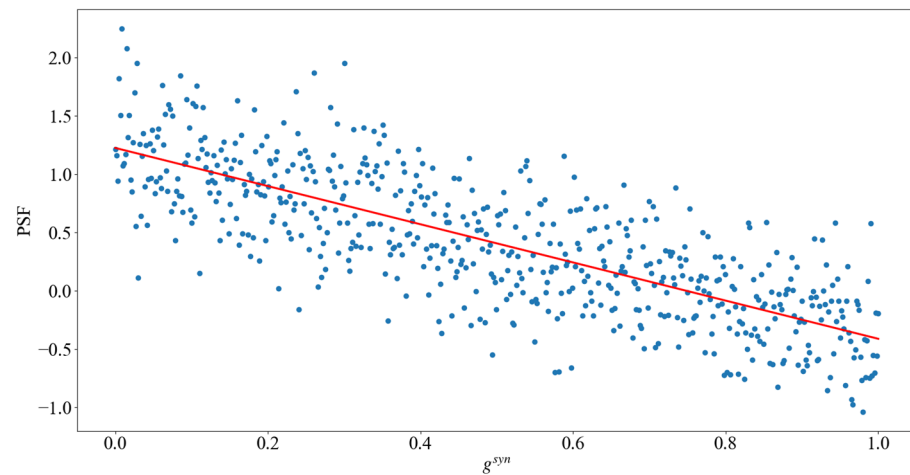


Figure 13. Synaptic strength on the change of PSF value.

The mechanism of information transmission between network nodes must have a success or failure state. In Equation (15), $PC(n_i, n_{i+1}, \Delta\varphi)$ is used to measure the success rate of information transmission between node pairs, where $\Delta\varphi$ denotes the coherence value of the phase deviation of the stimulus information passed between node pairs (n_i, n_j) , and to retain the link selection characteristics that the short path is better than the long path in the study process.

In addition, to determine the relationship between the information transmission path between a particular node pair $P_{i,j}$ and the offset phase $\Delta\varphi$ of the stimulus information, here, we give the preference selection index (pathway-phase-selectivity, PPS) of a specific pathway when the stimulus information carries different phase information, as defined in Equation (16):

$$PPS(p_m) = \max_{\Delta\varphi}(PA(p_m, \Delta\varphi)) - \min_{\Delta\varphi}(PA(p_m, \Delta\varphi)) \tag{16}$$

where $PPS(p_m)$ is determined by the activation state index PA of a path between node pairs. The PPS is used to measure the activation capability and transmission capability of a path given any path p_m between node pairs $P_{i,j}$ in the network with different phase information, i.e., $P_{i,j} = \{p_m | P_{i,j}, m \in N^*, i, j \in [0, n]\}$.

In addition, the selection strategy of the path with the largest transmission capacity between nodes is measured by using the phase information of the excitation signal, giving the quantitative index of the path selection mechanism (pathway-switching-selectivity, PSS), which is expressed in the form of (17):

$$PSS = \max_{P_{i,j}}(PA(p_1, \Delta\varphi_c) - PA(p_2, \Delta\varphi_c)) \tag{17}$$

where the PSS metric measures the stimulus phase difference at $\Delta\varphi_c$ and selects the path with optimal transmission capability in the path set $P_{i,j}$ between node pairs (n_i, n_j) . $P_{i,j}$ represents the path set between a pair of stimulus nodes n_i and n_j . It is assumed that p_1 represents the path with the strongest activation index in the path concentration PA , and p_2 represents the path of the second strongest activation index PA in the path concentration. In addition, when $PSS > 0$, it means that the p_1 path is more active in phase under the $\Delta\varphi_c$ condition, and when $PSS < 0$, it means that the p_2 path is more active.

In the process of analyzing the path activation index PA , all the paths between the five delay nodes are selected for evaluation, i.e., $P_{ij}, i, j \in [0, 5]$. The phase information carried by the stimulus information is used to modulate these node pairs, and then PA values under different phase offsets are calculated. Due to the existence of obvious or obscure phase relations, the simulation results are presented in polar coordinates. The radius in the figure indicates the magnitude of the PA value and the angle indicates the offset between different stimulus phases. The analysis is also performed for any of the

pathways in (n_1, n_5) for a given node, and the path selectivity index PPS is given to explore the phase dependence properties under a specific pathway.

The blue curve in Figure 14 indicates the path with the strongest PA between two node pairs, and the orange color indicates the second strongest path. For Figure 14a, the results show that both the strongest path PA value and the second strongest path PA value between a pair of nodes P_{15} are relatively stable and do not change significantly with the phase shift of the stimulus information. Figure 14b indicates that the strongest path PA value between node pair PA changes with the stimulus phase offset, indicating that the phase information carried by the stimulus information will have some influence on the PA value; that is, the phase information can be used to modulate the network and thus find the optimal path. Figure 14c shows that the strongest path and the second strongest path PA values between the nodes to P_{15} change almost together, i.e., it shows that the PA values will be modulated by the role of phase information, and the selection of the path by the information flow can be either of the two paths, indicating that both paths can characterize the information. Figure 14d shows that the phase information carried by the stimulus information in the node pair P_{15} has obvious modulation on the PA values of the strongest path and the second strongest path (blue in the figure indicates $\Delta\varphi \approx 1.5\pi$, orange indicates $\Delta\varphi \approx 0.5\pi$), which mainly shows that the strongest path and the second strongest path have a preferential choice of phase between them under different phase offsets, i.e., under different phase offsets of the stimulus information.

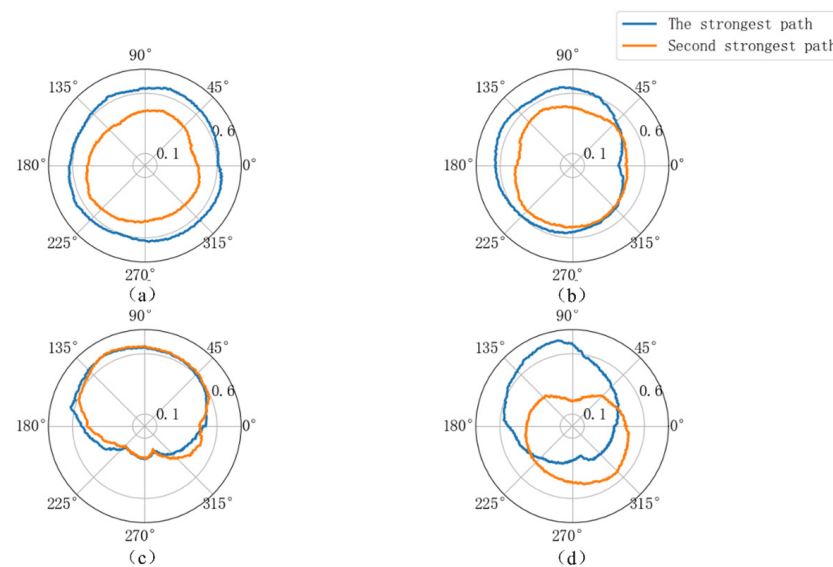


Figure 14. Path activation index PA under different phase shifts of stimulus information (a) Both the strongest and the second strongest paths are insensitive to phase. (b) Only the strongest path is phase sensitive. (c) The strongest and second strongest paths are sensitive to the same phase offset. (d) The strongest and second strongest paths are sensitive to different phase offsets.

When studying the path activation index PA , Figure 14 analyzes the relationship between the strongest path and the second strongest path with respect to the stimulus phase in the node (n_1, n_5) path set P_{15} . Based on this, it adopts the PPS to analyze any pathway in the path set P_{15} , and then explore the phase dependence of the specific pathway. Through the statistics of the data results, the PPS values of all node pairs in the network composed of five nodes are drawn, and the phase selectivity histogram is shown in Figure 15.

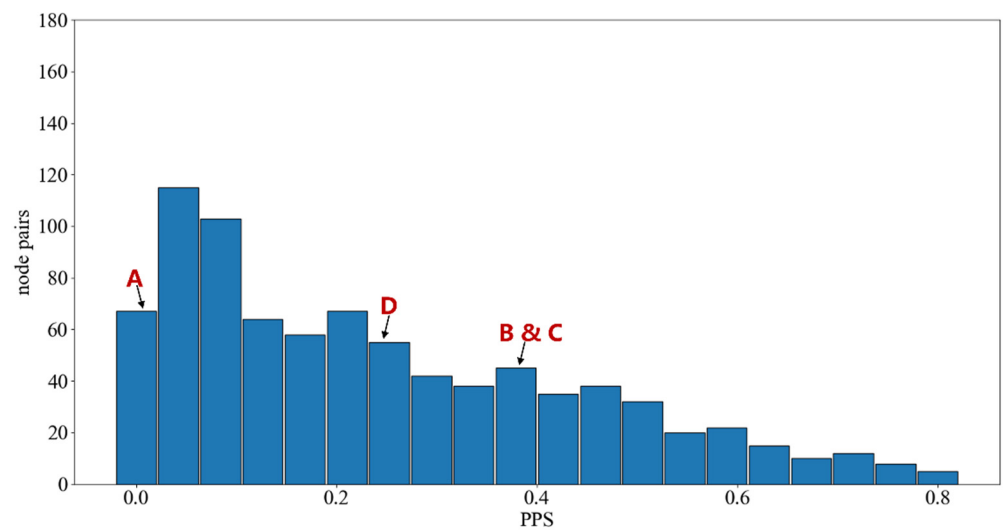


Figure 15. The Statistical Diagram of PPS of 180 nodes (A, B, C and D respectively corresponds to the four conditions in Figure 14.).

Figure 15 analyzes all paths between node pairs P_{15} . Statistical analysis of the data results is performed to plot the values of all node pairs between P_{15} . The results displayed are consistent with the conclusions of the theoretical analysis; that is, the larger value of PPS indicates that the path activation index is unstable and vulnerable to the modulation and influence of the phase information of the stimulus information. Figure 15 shows that the value of PPS is between 0 and 1, and the larger the value of PPS , the more the path between nodes are affected by the phase shift of the stimulus information. After counting the path values between 180 node pairs, A, B, C and D correspond to the subplots in Figure 14. It can be seen that when the change of PA value is small, the value of PPS is closer to 0, and when the change of PA value is larger, the value of PPS converges to 1. Through the statistical analysis, there exists a large number of paths between the network node pairs that all have the PPS effect, i.e., in a specific path state, they will have a certain preference depending on the phase information of the stimulus information, so this simulation shows that the phase information carried by the stimulus information can be used to determine the path based on the phase preference.

Theoretical analysis shows that in the information transmission, there should be nodes in the network to control the phase offset of the stimulated information so that they can preferentially choose a path as the main path of the network information flow transmission. i.e., as the optimal path to represent the information.

Therefore, this study gives the conditions under which the information flow will choose the path with the optimal information representation path (ORP) under the condition that the phase offset of the stimulus information is determined:

$$ORP = \max\{PSS(P_{i,j}, \Delta\varphi_c) | P_{i,j}, i, j \in [0, n]\} \tag{18}$$

where ORP denotes the strategy for selecting the optimal path between node pairs when the stimulus information phase $\Delta\varphi_c$ is perturbing the network. Its physical meaning indicates that in the path set of a pair of network node pairs, there must exist one or more optimal paths to enable them to have optimal transmission capability and more accurate characterization capability.

By analyzing the PPS values of the strongest path PA and the sub-strong path PA , it can be found that a large number of paths between the nodes have phase preference. Therefore, we next count the phase preference of the strongest path p_1 and the sub-strong path p_2 . The statistical histogram is shown in polar coordinates. The angle represents the phase shift of the stimulus information and the radius represents the frequency of path selection. The result is shown in Figure 16.

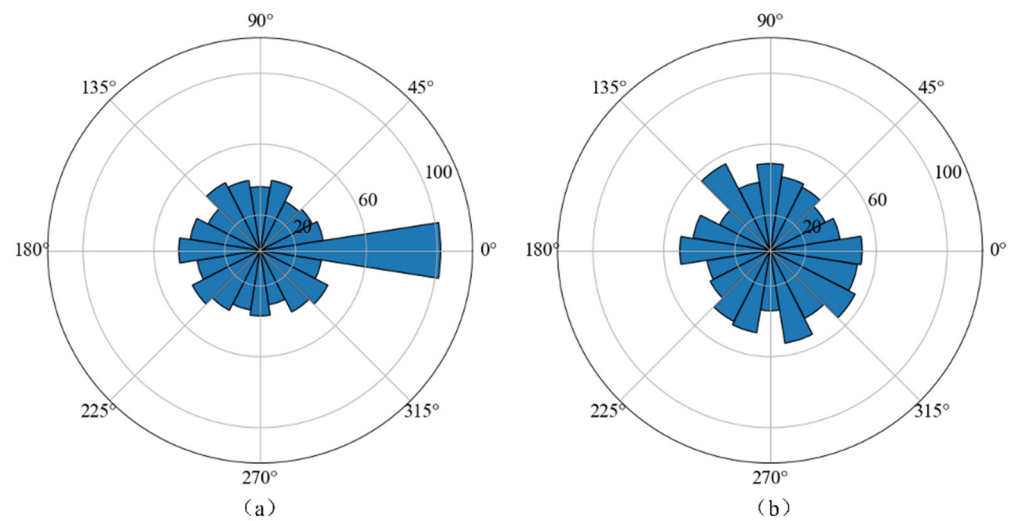


Figure 16. Histogram of path selection under specific phase conditions (a) The strongest path. (b) The sub-strong path.

Figure 16a shows the phase preference exhibited by the strongest path between a pair of nodes with phase shift, $\chi^2(20, 350) = 103.51$, $p < 0.001$, which is significantly different from the uniform distribution. It indicates that there is a significant peak at $\Delta\varphi = 0$, showing that the strongest path has a strong dependence on the phase information. Figure 16b shows the preference exhibited by the phase shift under the next strongest path, which is $\chi^2(20, 350) = 22.43$, $p = 0.035$ with some differences from the uniform distribution. Therefore, it can be found that the path with the strongest path activation index PA has a similar preference to the coherence PC between a pair of stimulated nodes, which indicates that using the phase information of the stimulus signal as a path selection switch for the information flow in the network is a feasible way. In addition, the present findings show that the phase offset of the stimulus information selects the path with the maximum transmission capacity (path activation index PA is maximum) when choosing the path, finding the optimal information representation loop. In other words, in brain-like intelligent networks, the functional loop can be switched by modulating the phase information carried by the stimulus information to achieve different functional tasks.

The phase preference between the strongest path and the second strongest path between any pair of nodes is analyzed in Figure 16. On this basis, we continue to count the PSS values of 180 node pairs (indifference filtering) under the disturbance of stimulus information with different phase differences in order to obtain the normalized path selection histogram between the strongest path and the second strongest path. By normalizing the square root of the PSS value, the simulation results in Figure 17 are obtained.

Figure 17 measures the modulation effect of phase information on the node-to-node paths by calculating the standard deviation of PSS . A , B , C and D in Figure 17 correspond to the subplots in Figure 14; when the value of PSS is positive, it means that the path switching index is low and the strongest path p_1 is more active, indicating that there is no need to choose other paths; when the value of PSS is negative, it means that the path switching index is high, and the optimal path can be switched by stimulus phase modulation.

In this study, through the analysis of all node pairs in a network of twenty nodes, it can be found that a significant portion of the paths between node pairs (about 42%) can be switched between the strongest path and the second strongest path by phase shifting of stimulus information. The simulation results indicate that such switching is one of the means of achieving structural robustness in the network and that a similar mechanism can be used in brain-like networks to accomplish the switching of functional loops and thus achieve optimal representation of information.

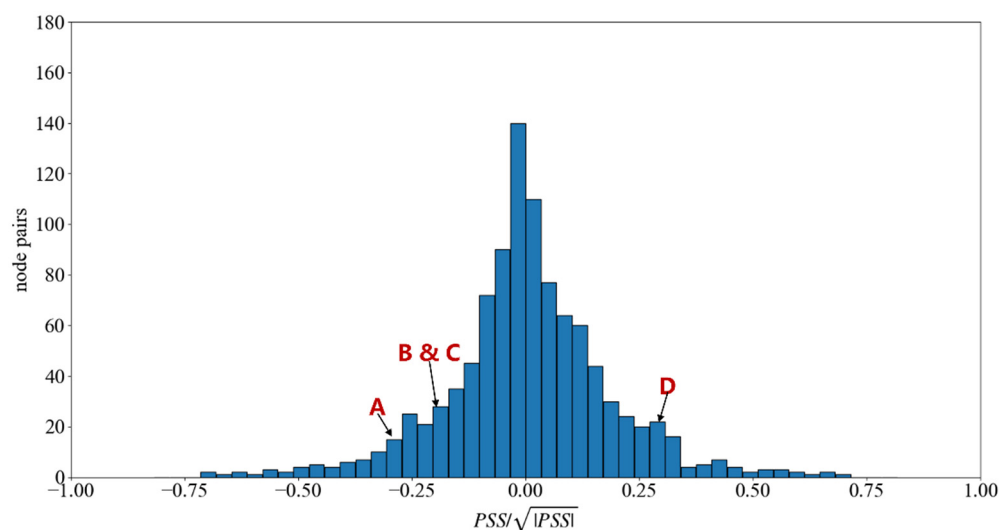


Figure 17. Path selectivity index PSS normalized histogram (A, B, C and D respectively corresponds to the four conditions in Figure 14.).

4. Conclusions

In conclusion, this paper constructs dynamic bionic synapses based on *ECM* concentration and applies them to the motif model. It then studies the close relationship between phase synchronization and effective links in brain networks, the regulation mechanism of dynamic path switching is explored scientifically, and the corresponding path evaluation index is given. In addition, based on the effects of transmission delay, synaptic strength and the number of central nodes on synchronization characteristics, a path selection method based on information flow disturbance is proposed and verified by statistical knowledge analysis; thus, it is proved that there is a regulatory relationship between the path selection mechanism and the phase difference of stimulus information in the network. The potential mechanism of efficient task-based brain networks is discussed based on the synchronization characteristics. This is of great significance to the realization of brain-like intelligence.

The development of brain-like intelligence is needed by the times, and the in-depth exploration of brain-like intelligence amounts to very meaningful work. This paper combines the latest research results of brain science to improve the construction of synaptic models. Synchronous state is used to study the potential mechanism of path selection in the network and verified by statistical analysis. However, there are still some shortcomings which need to be improved and perfected in future work. First of all, when studying the path selection mechanism, we develop an in-depth study from the phase information carried by the stimulus information, but the competitive relationship between the input signals is not taken into account. Secondly, in the network, with the regulation of stimulus information, brain-like networks will switch different paths. These paths can represent relevant information, but in the implementation of advanced activities, how to extract more accurate surface sign information is a question worth exploring in depth.

Author Contributions: Conceptualization, Y.C. and Y.H.; methodology, Y.C., Y.H. and Y.W.; software analysis, J.L. and A.L.; writing—original draft, J.L. and Y.W.; writing—review and editing, J.L., Y.H. and A.L. All authors have read and agreed to the published version of the manuscript.

Funding: This research received no external funding.

Institutional Review Board Statement: Not applicable.

Informed Consent Statement: Not applicable.

Data Availability Statement: Not applicable.

Conflicts of Interest: The authors declare no conflict of interest.

References

1. Mijatovic, G.; Lončar-Turukalo, T.; Bozanic, N.; Faes, L. Information–theoretic characterization of concurrent activity of neural spike trains. In Proceedings of the 28th European Signal Processing Conference, Amsterdam, The Netherlands, 18–21 January 2021; pp. 925–929.
2. Celik, M.E.; Balouji, E. Characterization of individual retinal ganglion cell responses using K-Means clustering method. In Proceedings of the International Artificial Intelligence and Data Processing Symposium, Malatya, Turkey, 16–17 September 2017; pp. 1–4.
3. Gontier, C.; Pfister, J.P. Identifiability of a Binomial Synapse. *Front Comput. Neurosci.* **2020**, *14*, 558477. [[CrossRef](#)] [[PubMed](#)]
4. Tabekoueng Njitacke, Z.; Sami Doubla, I.; Kengne, J.; Cheukem, A. Coexistence of firing patterns and its control in two neurons coupled through an asymmetric electrical synapse. *Chaos Interdiscip. J. Nonlinear Sci.* **2020**, *30*, 023101. [[CrossRef](#)] [[PubMed](#)]
5. Liu, Z.; Wang, C.; Zhang, G.; Zhang, Y. Synchronization between neural circuits connected by hybrid synapse. *Int. J. Mod. Phys. B* **2019**, *33*, 1950170. [[CrossRef](#)]
6. Dembitskaya, Y.; Gavrilo, N.; Kraev, I.; Doronin, M.; Tang, Y.; Li, L.; Semyanov, A. Attenuation of the extracellular matrix increases the number of synapses but suppresses synaptic plasticity through upregulation of SK channels. *Cell Calcium* **2021**, *96*, 102406. [[CrossRef](#)] [[PubMed](#)]
7. Shen, M.; Qu, Z.; DesLaurier, J.; Welle, T.M.; Sweedler, J.V.; Chen, R. Single Synaptic Observation of Cholinergic Neurotransmission on Living Neurons: Concentration and Dynamics. *J. Am. Chem. Soc.* **2018**, *140*, 7764–7768. [[CrossRef](#)]
8. Wang, L.; Zhang, J.; Liu, T.; Chen, D.; Yang, D.; Go, R.; Wu, J.; Yan, T. Prediction of Cognitive Task Activations via Resting-State Functional Connectivity Networks: An EEG Study. *IEEE Trans. Cogn. Dev. Syst.* **2022**, *14*, 181–188. [[CrossRef](#)]
9. Guo, A. A cross-species review of cognitive neural circuits to illuminate the way to brain-inspired intelligence. *Sci. Sin. Vitae* **2019**, *49*, 1354.
10. Zhou, Z. *Study on the Neural Circuitry Regulation Mechanism of Instinctive Fear*; University of Chinese Academy of Sciences, Shenzhen Advanced Technology Research Institute: Shenzhen, China, 2018.
11. Aljadeff, J.; Gillett, M.; Pereira Obilinovic, U.; Brunel, N. From synapse to network: Models of information storage and retrieval in neural circuits. *Curr. Opin. Neurobiol.* **2021**, *70*, 24–33. [[CrossRef](#)]
12. Pereda, A.E. Electrical synapses and their functional interactions with chemical synapses. *Nat. Rev. Neurosci.* **2014**, *15*, 250–263. [[CrossRef](#)]
13. Magee, J.C.; Grienberger, C. Synaptic Plasticity Forms and Functions. *Annu. Rev. Neurosci.* **2020**, *43*, 95–117. [[CrossRef](#)]
14. Mannan, Z.I.; Kim, H.; Chua, L. Implementation of Neuro-Memristive Synapse for Long-and Short-Term Bio-Synaptic Plasticity. *Sensors* **2021**, *21*, 644. [[CrossRef](#)] [[PubMed](#)]
15. Mannan, Z.I.; Adhikari, S.P.; Yang, C.; Budhathoki, R.K.; Kim, H.; Chua, L. Memristive Imitation of Synaptic Transmission and Plasticity. *IEEE Trans. Neural. Netw. Learn. Syst.* **2019**, *30*, 3458–3470. [[CrossRef](#)] [[PubMed](#)]
16. Honey, C.J.; Kötter, R.; Breakspear, M.; Sporns, O. Network structure of cerebral cortex shapes functional connectivity on multiple time scales. *Proc. Natl. Acad. Sci. USA* **2007**, *104*, 10240–10245. [[CrossRef](#)] [[PubMed](#)]
17. Coito, A.; Michel, C.M.; Vulliemoz, S.; Plomp, G. Directed functional connections underlying spontaneous brain activity. *Hum. Brain Mapp.* **2019**, *40*, 879–888. [[CrossRef](#)] [[PubMed](#)]
18. Lazarevich, I.; Stasenko, S.; Rozhnova, M.; Pankratova, E.; Dityatev, A.; Kazantsev, V. Activity-dependent switches between dynamic regimes of extracellular matrix expression. *PLoS ONE* **2020**, *15*, e0227917. [[CrossRef](#)]
19. Kazantsev, V.; Gordleeva, S.; Stasenko, S.; Dityatev, A. A homeostatic model of neuronal firing governed by feedback signals from the extracellular matrix. *PLoS ONE* **2012**, *7*, e41646. [[CrossRef](#)]
20. Lin, Q.; Rosenberg, M.D.; Yoo, K.; Hsu, T.W.; O’Connell, T.P.; Chun, M.M. Resting-State Functional Connectivity Predicts Cognitive Impairment Related to Alzheimer’s Disease. *Front. Aging Neurosci.* **2018**, *10*, 94. [[CrossRef](#)]
21. Fornito, A.; Zalesky, A.; Bullmore, E. *Fundamentals of Brain Network Analysis*; Academic Press: Cambridge, MA, USA, 2016.
22. Plakke, B.; Romanski, L.M. Neural circuits in auditory and audiovisual memory. *Brain Res.* **2016**, *1640*, 278–288. [[CrossRef](#)]
23. Stampanoni Bassi, M.; Iezzi, E.; Gilio, L.; Centonze, D.; Buttari, F. Synaptic Plasticity Shapes Brain Connectivity: Implications for Network Topology. *Int. J. Mol. Sci.* **2019**, *20*, 6193. [[CrossRef](#)]
24. Lynn, C.W.; Bassett, D.S. The physics of brain network structure, function and control. *Nat. Rev. Phys.* **2019**, *1*, 318–332. [[CrossRef](#)]
25. Sherrington, C.S. The Integrative Action of the Nervous System. *Nature* **1907**, *76*, 122.
26. Benedetto, A.; Lozano-Soldevilla, D.; VanRullen, R. Different responses of spontaneous and stimulus-related alpha activity to ambient luminance changes. *Eur. J. Neurosci.* **2018**, *48*, 2599–2608. [[CrossRef](#)]
27. Novembre, G.; Pawar, V.M.; Kilintari, M.; Bufacchi, R.J.; Guo, Y.; Rothwell, J.C.; Iannetti, G.D. The effect of salient stimuli on neural oscillations, isometric force, and their coupling. *Neuroimage* **2019**, *198*, 221–230. [[CrossRef](#)] [[PubMed](#)]
28. Bauer, A.R.; Bleichner, M.G.; Jaeger, M.; Thorne, J.D.; Debener, S. Dynamic phase alignment of ongoing auditory cortex oscillations. *Neuroimage* **2018**, *167*, 396–407. [[CrossRef](#)] [[PubMed](#)]
29. Yu, S.; Zheng, N.; Ma, Y.; Wu, H.; Chen, B. A Novel Brain Decoding Method: A Correlation Network Framework for Revealing Brain Connections. *IEEE Trans. Cogn. Dev. Syst.* **2019**, *11*, 95–106. [[CrossRef](#)]
30. Zimmermann, J.; Griffiths, J.D.; McIntosh, A.R. Unique Mapping of Structural and Functional Connectivity on Cognition. *J. Neurosci.* **2018**, *38*, 9658–9667. [[CrossRef](#)]

31. Izhikevich, E.M. *Dynamical Systems in Neuroscience: The Geometry of Excitability and Bursting*; The MIT Press: Cambridge, MA, USA, 2006.
32. Izhikevich, E.M.; FitzHugh, R. Fitzhugh45nagumo model. *Scholarpedia* **2006**, *1*, 1349. [[CrossRef](#)]

Disclaimer/Publisher's Note: The statements, opinions and data contained in all publications are solely those of the individual author(s) and contributor(s) and not of MDPI and/or the editor(s). MDPI and/or the editor(s) disclaim responsibility for any injury to people or property resulting from any ideas, methods, instructions or products referred to in the content.